Journal of the Mechanical Behavior of Biomedical Materials 95 (2019) 116–123

Contents lists available at ScienceDirect

Journal of the Mechanical Behavior of Biomedical Materials

journal homepage: www.elsevier.com/locate/jmbbm

A combined experimental-numerical lamellar-scale approach of tensile rupture in arterial medial tissue using X-ray tomography

J. Brunet[a,*], B. Pierrat[a], E. Maire[b], J. Adrien[b], P. Badel[a]

[a] Mines Saint-Etienne, Univ Lyon, Univ Jean Monnet, INSERM, U 1059 Sainbiose, Centre CIS, F-42023, Saint-Etienne, France
[b] Université de Lyon, INSA-Lyon, MATEIS CNRS UMR5510, Villeurbanne, France

ARTICLE INFO

Keywords:
Aortic dissection
Cohesive zone
Rupture
Finite element model
Delamination

ABSTRACT

Aortic dissection represents a serious cardio-vascular disease and life-threatening event. Dissection is a sudden delamination event of the wall, possibly leading to rupture within a few hours. Current knowledge and practical criteria to understand and predict this phenomenon lack reliable models and experimental observations of rupture at the lamellar scale. In an attempt to quantify rupture-related parameters, the present study proposes an analytical model that reproduces a uniaxial test on medial arterial samples observed under X-ray tomography. This model is composed of several layers that represent the media of the aortic wall, each having proper elastic and damage properties. Finite element models were created to validate the analytical model using user-defined parameters. Once the model was validated, an inverse analysis was used to fit the model parameters to experimental curves of uniaxial tests from a published study. Because this analytical model did not consider delamination strength between layers, a finite element model that included this phenomenon was also developed to investigate the influence of the delamination on the stress-strain curve through a sensitivity analysis. It was shown that shear delamination strength between layers, i.e. mode II separation, is essential in the rupture process observed experimentally.

Statement of significance

Most of existing models investigating aortic dissection phenomena are at the macro-scale. In this work, we propose a lamellar-scale rupture model based on published experiments. The model reproduces the experimental data with great accuracy and provides rupture values for layers of the media and for delamination between these layers, which are still scarce in the literature. Thus, this study provides a better understanding of the rupture mechanism involved in aortic dissection.

1. Introduction

Aortic dissection, a sudden delamination of the aortic wall in its medial layer, is a life-threatening arterial event associated with a very poor outcome, and requires rapid diagnosis and decision-making; without intervention, up to 90% of patient with acute aortic dissection die within weeks (Kouchoukos and Dougenis, 1997). As highlighted by the review of Nienaber et al. (2016), dissection is usually thought to be caused by an intimal tear in which the blood rushes and propagates in the medial layer. Dissection can also be initiated at the site of an intramural hemorrhage, which is thought to be less frequent. Aortic dissection has an incidence of 35 cases per 100,000 people per year in the 65-75 year-old age group. Hypertension, dyslipidaemia and genetic disorders like the Marfan syndrome are known risk factors.

Despite its high mortality, few studies have tried to explain the microstructural phenomena occurring during initiation and propagation of dissection in the aorta. Advanced mechanical analyses of the underlying mechanisms, based on mechanical experiments as well as structural observations at the micro- and meso-scales – these two being possibly combined – would deeply improve the understanding of such fatal event and could improve clinical decision-making criteria.

Regarding the architecture of the tissue, the medial layer is a complex structure consisting of several lamellar units separated by elastic laminae [25]. Each unit is mainly composed of elastin, collagen and smooth muscle cells. Due to its organization, the media is weaker in the radial direction, compared to the axial and circumferential directions (MacLean et al., 1999). Thus, it is prone to dissection separation.

Previous scientific work mainly involved macro-scale testing. Roach and co-workers infused a fluid into the media at a constant flow, while recording pressure and volume, in order to investigate the mechanisms leading to aortic dissection (Carson and Roach, 1990). The measurements showed that the peak pressure needed to dissect the aortic media

* Corresponding author. Centre Ingénierie et Santé École Nationale Supérieure des Mines 10 Rue de la Marandière, 42270, Saint-Priest-en-Jarez, France.
E-mail address: joseph.brunet@emse.fr (J. Brunet).

https://doi.org/10.1016/j.jmbbm.2019.03.028
Received 3 December 2018; Received in revised form 26 March 2019; Accepted 27 March 2019
Available online 01 April 2019
1751-6161/

was 77.2 ± 1.5 kPa and the energy release rate needed to propagate the dissection was 15.9 ± 0.9 mJ/cm^2. Another study focused on radial tensile and peeling tests to quantitatively assess the properties of the medial layer (Sommer et al., 2008). The results showed that the energy release rates measured in peeling were 5.1 ± 0.6 mJ/cm^2 in the circumferential direction and 7.6 ± 2.7 mJ/cm^2 in the longitudinal direction; the difference was explained by the alignment of components like collagen fibers and smooth muscle cells.

In regard to imaging techniques allowing the investigation of the microstructure of arterial wall, multiphoton microscopy is widely used. This technique enables the observation of the sample at fiber-scale (with a resolution of about one micron) but it is limited by a small volume of observation (approximately 500 × 500 × 200 μm^3) (Krasny et al., 2017). Some groups have used X-ray tomography to investigate the microstructural architecture of vascular soft tissues. Phase contrast techniques provides a good resolution and contrast with a wide field of view; however, samples have to be embedded and the time required to obtain images is extremely long, preventing *in situ* testing (Walton et al., 2015). Some authors compared different contrast agents to observe microstructural components like collagen, but the samples were unloaded (Nierenberger et al., 2015).

In a previous study, an X-ray tomography experiment taking advantage of the versatility of the technique to perform *in situ* tensile testing was developed. Using a specific staining technique and a specific tensile machine, this study provided unprecedented observations of medial tissue under tension, and a meso-scale description of medial rupture, possibly constituting a model for *in vitro* dissection (Helfenstein-Didier et al., 2018).

In the context of aortic dissections, modeling rupture has been a challenge and only a few models have been published in the literature. Gasser and Holzapfel (2006) developed a non-linear continuum framework composed of a continuous material and a cohesive material. The continuous material was modeled as a fiber-reinforced composite with collagen fibers embedded in a non-collagenous isotropic ground matrix. The two materials were independent from each other. The framework was then implemented in a finite element model to reproduce a peeling test and investigate the propagation of arterial dissection. Ferrara and Pandolfi (2010) presented a numerical model of dissection based on cohesive fracture theory. The model was implemented in a numerical simulation of a peeling test. A sensitivity analysis was then performed to evaluate the influence of the cohesive parameters driving the interlamellar propagation of the dissection in the media and the influence of the reinforcing collagen fibers on the separation of the layers. Wang et al. (2015) proposed a computational model to study the propagation of a tear in a fiber-reinforced tissue. The energy release rate was calculated, allowing them to determine the values of pre-existing tear length and internal pressure needed to propagate the tear. The effect of fiber orientation and surrounding connective tissues were also investigated. Later, Wang et al. (2017) developed a residually stressed two-layer arterial model. The material properties were modeled using the Gasser-Ogden-Holzapfel model, and the propagation of the tear was described with a linear traction-separation law. The extended finite element method was used for the simulation. The effect of residual stresses in the arterial wall on the dissection propagation was investigated. Notably, these models studied dissection at the scale of the whole wall. For a better understanding of the phenomena involved in this disease, a lamellar-scale model is needed.

The present study aimed at characterizing and quantifying the mechanisms triggering and propagating a dissection in medial tissue. To this aim, an analysis of the previously published experimental work (Helfenstein-Didier et al., 2018) is proposed based on analytical and numerical approaches using linear cohesive models, first introduced by Dugdale and Barrenblatt (Barenblatt, 1962; Dugdale, 1960), and as often used in commercial codes to model crack opening and rupture. The approach was used to identify the cohesive model's parameters, which were later used in a finite element (FE) model to assess the relative influence of different crack propagation modes in the tissue.

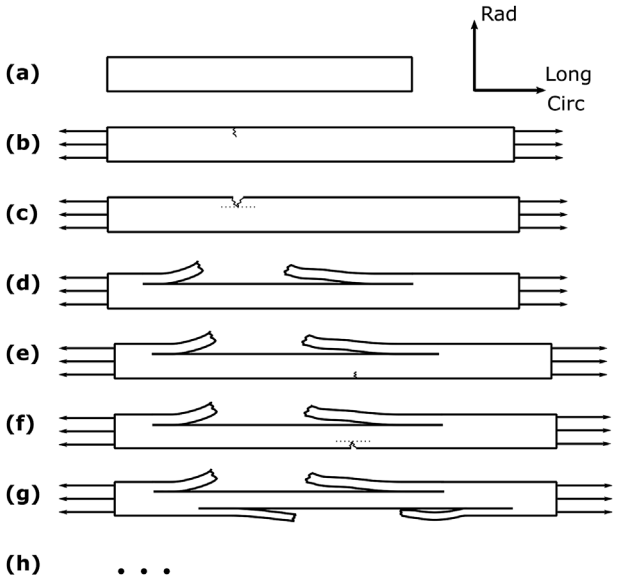

Fig. 1. Schematic representation of the damage initiation and propagation mechanism observed *in situ*. (a) intact sample, (b and c) initial radial crack, opening in mode I, (d) elastic recoil of the ruptured layers, causing a mode II longitudinal crack to form and propagate, (f, g, h …) the process repeats until complete failure of the sample. Modified from Helfenstein-Didier et al. (2018).

2. Methods

2.1. Experimental data

In a previously published experimental study (Helfenstein-Didier et al., 2018), uniaxial rupture tests were performed *in situ* on medial layers of porcine aortic samples under X-ray micro-tomography. Briefly, the technique required the use of sodium polytungstate as a contrast agent, applied by immersing the samples in such a solution. This made it possible to image the lamellar units in the tissue when performing 3D scans of the samples. X-ray micro-tomography provided a mean to monitor damage initiation, delamination and rupture of medial tissue under tensile loading. The process was described as an elementary process repeating several times until complete failure. This elementary process initiated with a sudden mode I fracture (in the loading direction) of a group of lamellar units, followed by an elastic recoil of these units, causing mode II separation creating a delamination plane as shown in Fig. 1.

To build dissection models and identify their parameters, the qualitative observations made during the tensile tests performed up to rupture were used, along with the force-displacement curves obtained at the same time. Ten samples and their corresponding data were used in the present study.

2.2. Analytical multi-layer cohesive model

A 1D analytical model was created to numerically reproduce the uniaxial test responses of medial tissue. The dimensions taken into account (length, thickness and width of the rectangular samples) were obtained from the X-ray tomography images (Helfenstein-Didier et al., 2018). The model was composed of several layers in parallel, all layers were assumed to have the same dimensions. Each layer represented a group of several lamellar units, the number of groups was determined based on the traction curve, as detailed in section 2.3 below. The behavior of each layer was governed by an incompressible hyperelastic contribution and a cohesive contribution, both assumed to work in

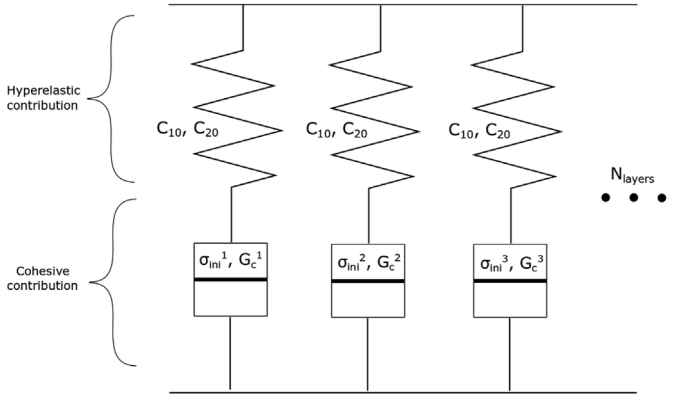

Fig. 2. Schematic representing the analytical model and its material parameters.

series (see Fig. 2). Note that this 1D model, can only include mode I fracture; mode II will be addressed later in the proposed FE model.

Because the model primarily aims at studying the response at rupture, the medial tissue was assumed to have an isotropic mechanical behavior for the hyperelastic contribution which was modeled with an incompressible second order reduced polynomial constitutive equation (Rivlin, 1948). The strain energy function of this model was defined as:

$$\Psi = C_{10}(\bar{I}_1 - 3) + C_{20}(\bar{I}_1 - 3)^2, \quad \text{(Eq. 1)}$$

with C_{10} and C_{20} the material parameters and $\bar{I}_1$ the first deviatoric strain invariant defined as $\bar{I}_1 = tr\ \bar{C}$. $\bar{C} = \bar{F}^t\bar{F}$ is the deviatoric right Cauchy-Green tensor and $\bar{F}$ is the deviatoric part of the deformation gradient tensor.

The specificity of this analytical model of the media was to also include a cohesive part in each layer. The objective was to reproduce the damage initiation and evolution until total rupture observed during the uniaxial tests. The motivation to use independent cohesive interfaces in each layer was that layers, comprising several lamellar units, were observed not to break at the same time in our previous uniaxial tests (Helfenstein-Didier et al., 2018). It was assumed that the cause of this phenomenon was the presence of defects in the layers. Thus, to reproduce different defects with different possible rupture thresholds, cohesive interfaces were introduced, in series with the hyper-elastic material. In this model, the global strain is equal to the strain in each layer, and the global force is the sum of the contributions from all layers. The response of a cohesive interface is illustrated in Fig. 3. Only

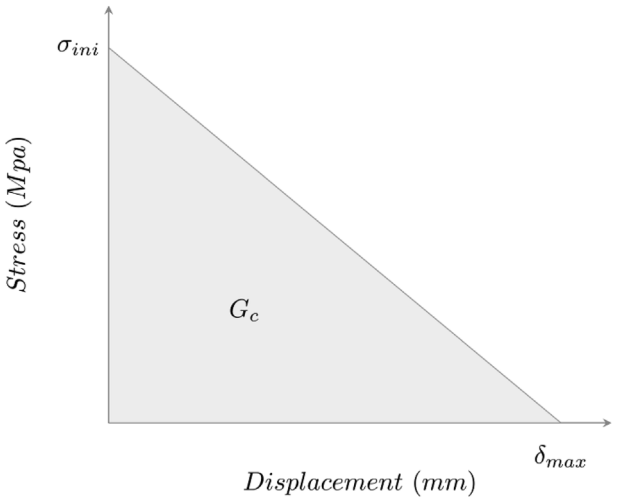

Fig. 3. Cohesive behavior with the stress as a function of the opening of the crack.

traction (related to mode I of rupture) was taken into account in this 1D model. Damage begins when the damage initiation criterion is met:

$$max\left[\frac{\sigma}{\sigma_{ini}}\right] = 1, \quad \text{(Eq. 2)}$$

where σ (MPa) is the normal stress in the normal direction (ie. the loading direction here) and σ_{ini} is the damage initiation stress which represents the peak value of the normal stress. Damage evolution was defined by a decreasing linear law which describes the rate of degradation of the cohesive zone stiffness. This law was defined based on the fracture energy Gc which is the amount of energy dissipated during the complete rupture of the cohesive zone. The choice of this cohesive zone model was motivated by the study of Miao et al. (2018), which compared the effects of four types of cohesive zone model shapes: triangular, trapezoidal, linear-exponential and exponential-linear, on the predictability of arterial wall failure. The results indicated that triangular and exponential-linear cohesive zone models were able to reproduce the aortic tissue failure behavior well, justifying the choice of the simplest model in this study.

In summary, the constitutive response of the model under uniaxial tension was governed by the following parameters:

- C_{10} and C_{20}, the material parameters defining the hyperelastic behavior. They were identified by an inverse curve-fitting method (see next section).
- σ_{ini}, the damage initiation stress. In the present model, there were as many damage initiation criteria as layers. They were set manually based on the uniaxial tension curves.
- G_c, the critical fracture energy and is defined as the area under the damage part of the cohesive response curve (Fig. 3). There were as many critical fracture energies as layers. They were identified using an inverse method (see section 2.3).
- N_{layer}, the number of layers present in the analytical model (typically 1 to 5).

Using a Matlab® code, nominal stress and nominal strain were calculated in each layer and the stress-strain curve of the whole model was obtained. The next steps were (i) to validate the implementation of the model (see next paragraph), and (ii) propose a strategy to identify the parameters of the model based on experimental tensile curves (see next section).

2.2.1. Model implementation validation

To validate the implementation of the analytical model, two finite element models were built in Abaqus®. The first model consisted of a single layer and the second model of two layers. The same dimensions were used in the analytical model and the finite element models. Cohesive zones were placed at the center of each layer to allow rupture in traction. The hyperelastic and cohesive parameters were set at the same values for the finite element and analytical models. Arbitrary, but realistic, fixed parameters were used. The stress-strain curves of both models were compared and the coefficients of determination, r^2, were calculated.

2.3. Inverse parameter identification

The following step of this study was an inverse analysis to obtain the set of parameters fitted to the experimental curves. The method was based on an cost function which quantifies the difference between the result of the simulation and the experimental data, and on an optimization algorithm which finds the parameters minimizing this function. The algorithm used here was described in Lagarias et al. (1998), and was programmed within an in-house Matlab® code. Because the developed model involved many parameters to be identified for each curve, a global optimization on the whole curve would have given non-

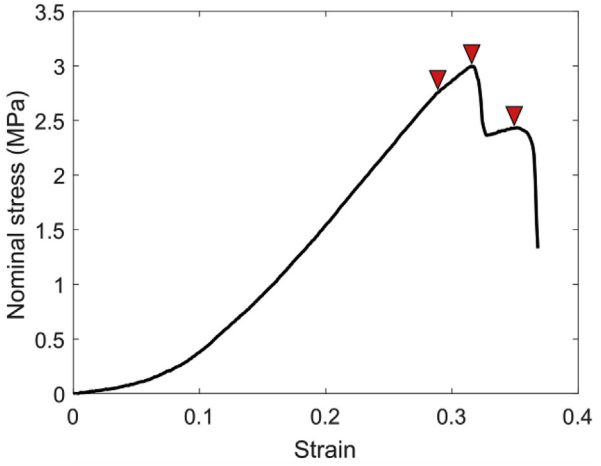

Fig. 4. Example of experimental stress-strain curve, with manually selected damage initiation points (represented by the arrows).

unique solutions. Instead, a three-step strategy based on separating the elastic response and the post-damage initiation response was used, and the damage initiation stresses were directly identified.

The first step aimed at identifying hyperelastic parameters C_{10} and C_{20}. The cost function used in the optimization algorithm was defined as follows:

$$Cost\ Function = \sum_{1}^{N} \frac{(\sigma_{num} - \sigma_{exp})^2}{N}, \quad \text{(Eq. 3)}$$

where σ_{num} and σ_{exp} were the model and experimental stress values at the n^{th} point, respectively. N was the total number of points in the range of strain observed experimentally on the stress-strain curves. Only the undamaged part of the experimental curve (i.e. before any discontinuity in the slope) was used for this identification.

The second step of the method consisted in a direct identification of the different damage initiation stresses. This was performed by the manual selection of break points in the slope of the experimental curves (an example is shown Fig. 4), considering that break points correspond to the rupture of one or multiple layers.

Last, the third step consisted in an inverse identification of the critical fracture energies of each cohesive zone (there was one cohesive zone per layer). To this aim, the same cost function as defined in Eq. (3) was used, with n varying in the range of strain beyond elastic strain. This identification provided the last set of parameters needed to completely define the model.

2.4. FE model to study the influence of mode II separation

During *in vitro* tensile tests, it was observed that layers initially break in mode I and then separate from each other, in mode II (Helfenstein-Didier et al., 2018). The analytical model presented above was suitable to identify the rupture parameters in mode I but did not allow for the identification of the parameters related to mode II. Thus, a 2D FE model that included delamination between layers was created using Abaqus®. Its dimensions were kept the same as those of the analytical model. Cohesive zones were defined (i) in the middle of each layer, in the transverse direction, to account for mode I separation, and (ii) between layers, parallel to the loading direction, to account for mode II separation which was not included in the analytical model. Mode I cohesive properties of each layer were taken from the previous analysis, but the weakest one was always chosen on the intimal side as observed experimentally (Helfenstein-Didier et al., 2018). Regarding mode II, a sensitivity analysis was performed to assess the influence of mode II initiation criterion and fracture energy. Uniaxial tension boundary conditions were applied. The mesh was comprised of 600 CPS4 elements (four-node plane stress element) and the quasi-static problem was solved using the implicit solver of Abaqus®.

3. Results

3.1. Verification

The results of the verification of the analytical model against a finite element implementation are presented in Fig. 5 for the one-layer model (Fig. 5a) and the two-layer model (Fig. 5b). The comparison was focused on the nominal stress as a function of the total strain of the specimen. In this work, only the nominal strain was considered.

The different parameters used in the verification are presented in Table 1. For the one-layer model, the coefficient of determination r^2 was 0.997 and for the two-layer model, 0.994, confirming proper implementation of the analytical model.

3.2. Inverse identification of hyperelastic and cohesive parameters

Table 2 provides the values of all the parameters obtained following the three-step identification procedure detailed in Section 2.3, for 10 experimental specimens tested in Helfenstein-Didier et al. (2018).

The comparisons between the analytical model and experimental tensile test stress-strain curves exhibited a good quantitative agreement

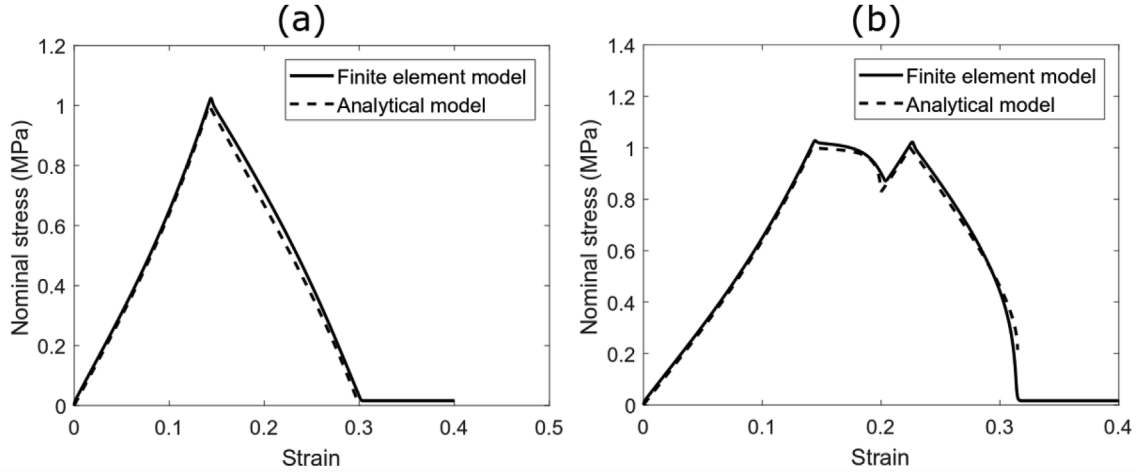

Fig. 5. Responses of analytical model (dashed curve) and finite element model (solid curve) with (a) one layer and (b) two layers, with the two peaks corresponding to each layers damaging successively.

Table 1
Parameters used during the verification with the one-layer model and the two-layer model.

	C_{10} (MPa)	C_{20} (MPa)	σ_{ini} (MPa)	G_c (MPa.mm)
Model with one layer				
Layer 1	1	3	1	3
Model with two layers				
Layer 1	1	3	1	2
Layer 2	1	3	2	6

considering that the r^2 values were in a range of 0.97–0.99 (Fig. 6). It can be observed that the global shape of the curves was well reproduced by the model although the smallest slope-breaks were neglected.

A comparison between the experimental images from one test and the model is presented in Fig. 7. The parameters of the model were identified from the corresponding stress-strain curve. In the first step, one can observe the undamaged media, then a first rupture on the intimal side corresponding to a change in slope on the stress-strain curve, followed, in the third step, by a second rupture on the adventitial side of the media and finally, in the fourth step, the remaining part of the media damaging before complete rupture. Note that, in the last step, the middle layer is in a partial damage state where δ_{max} has not been reached yet (Fig. 3). The finite element model shows a good qualitative agreement with the X-ray images.

3.3. FE model to study the influence of mode II

The stress-strain curves obtained from the finite element simulations including mode II separation in longitudinal cohesive zones are shown in Fig. 8. The parameters of mode II used for the simulation are displayed on the graphs.

The simulation showed that, if the mode II damage initiation stress was increased in the longitudinal cohesive zone, the two adjacent layers of this zone would not separate. Instead, they formed a single unit where the strongest layer (not broken in mode I) supported the weakest one (already broken in mode I) and prevented its elastic recoil. Both layers would recoil later, at the same time, when the strongest one failed in mode I. This phenomenon can be seen from the dashed curve in Fig. 8a where the global resistance of the model was increased but the rupture was sudden. The latter observation would contradict the experimental observations, which suggests that the resistance to mode II separation in the longitudinal direction is probably one of the most influential factors in dissection-like propagation. Note however, that the mode II critical fracture energy was found to have a relatively low influence on the model response (Fig. 8b).

4. Discussion

This paper follows up on a series of experimental uniaxial tests made on porcine medial aorta samples under X-ray tomography (Helfenstein-Didier et al., 2018). These tests observed the media at the lamellar-scale during damage progression and rupture and showed that layers (i.e. a group of lamellar units) successively break in tension (mode I) followed by a sudden delamination due to their elastic recoil (mode II separation). These findings motivated this study aiming at further understanding and quantifying these phenomena. An analytical model was developed with the objective of reproducing the uniaxial tests and identifying the different parameters in each layer relative to rupture.

The implementation of the model was numerically verified against a finite element model based on the same assumptions and parameters. Subsequently, all parameters of the model were successfully identified for each available experimental curve with the method described herein. It is worth noting that these results did not differ when repeating the procedure several times on the same experimental curves, showing the robustness of the method, even if part of this method remains operator-dependent since the damage initiation stresses are set manually.

For all experimental samples, the damage initiation stress and the critical fracture energy were obtained for a finite number of layers (structurally, these layers include several lamellar units). The values of damage initiation stresses are in the range of maximum stresses found in literature (750 kPa–2500 kPa (Wolinsky and Glagov, 1967)). Regarding the critical fracture energy, it can be noted that a marked variability between the different samples was obtained, which is mainly attributable to the variability of the curves themselves as reported by Helfenstein-Didier et al. (2018). Nevertheless, our study is, to the best of our knowledge, the first to report experimentally-supported values of mode I critical fracture energy at the lamellar-scale of aortic medial tissue. They can serve as a basis to the development of numerical models of arterial damage.

Because the analytical model did not take into account mode II strength and separation of different layers, a finite element model was built which included this phenomenon between layers. The same values

Table 2
Parameters obtained for all experimental curves.

Test number	C_{10} (MPa)	C_{20} (MPa)	σ_{ini} 1 (MPa)	σ_{ini} 2 (MPa)	σ_{ini} 3 (MPa)	σ_{ini} 4 (MPa)	σ_{ini} 5 (MPa)	G_c 1 (MPa.mm)	G_c 2 (MPa.mm)	G_c 3 (MPa.mm)	G_c 4 (MPa.mm)	G_c 5 (MPa.mm)
1	0.00103	0.181	0.815	0.815	0.871	1.045		2.40	2.40	3.48	3.41	
			0.887 ± 0.109 MPa					2.92 ± 0.602 MPa mm				
2	0.758	3.06	2.81	3.44	4.30			6.61	9.24	9.08		
			3.52 ± 0.744 MPa					8.31 ± 1.48 MPa mm				
3	1.64	1.03	2.75	3.00	3.32			9.98	10.7	11.0		
			3.02 ± 0.283 MPa					10.6 ± 0.543 MPa mm				
4	0.125	0.0705	0.543	0.750	0.750	0.800	0.800	2.70	3.57	3.57	1.84	1.84
			0.729 ± 0.107 MPa					2.92 ± 0.832 MPa mm				
5	0.210	0.0474	0.299	0.319	0.774	0.848		0.574	2.32	4.87	4.57	
			0.560 ± 0.291 MPa					3.09 ± 2.02 MPa mm				
6	0.175	0.0331	0.686	0.742	0.759	0.759		4.52	4.19	1.93	1.93	
			0.737 ± 0.0345 MPa					3.15 ± 1.41 MPa mm				
7	0.184	0.0943	0.484	0.522	0.845	0.990	0.990	1.68	3.65	4.74	4.56	4.56
			0.766 ± 0.248 MPa					3.66 ± 1.40 MPa mm				
8	0.196	0.00170	0.567					3.76				
9	0.140	0.0574	0.484	0.524	0.549			2.37	2.09	1.029		
			0.519 ± 0.0326 MPa					1.83 ± 0.706 MPa mm				
10	0.0744	0.0988	0.434	0.747	0.820			1.62	3.25	3.025		
			0.667 ± 0.205 MPa					2.63 ± 0.884 MPa mm				
Mean σ_{ini} 1 (MPa)			0.988									

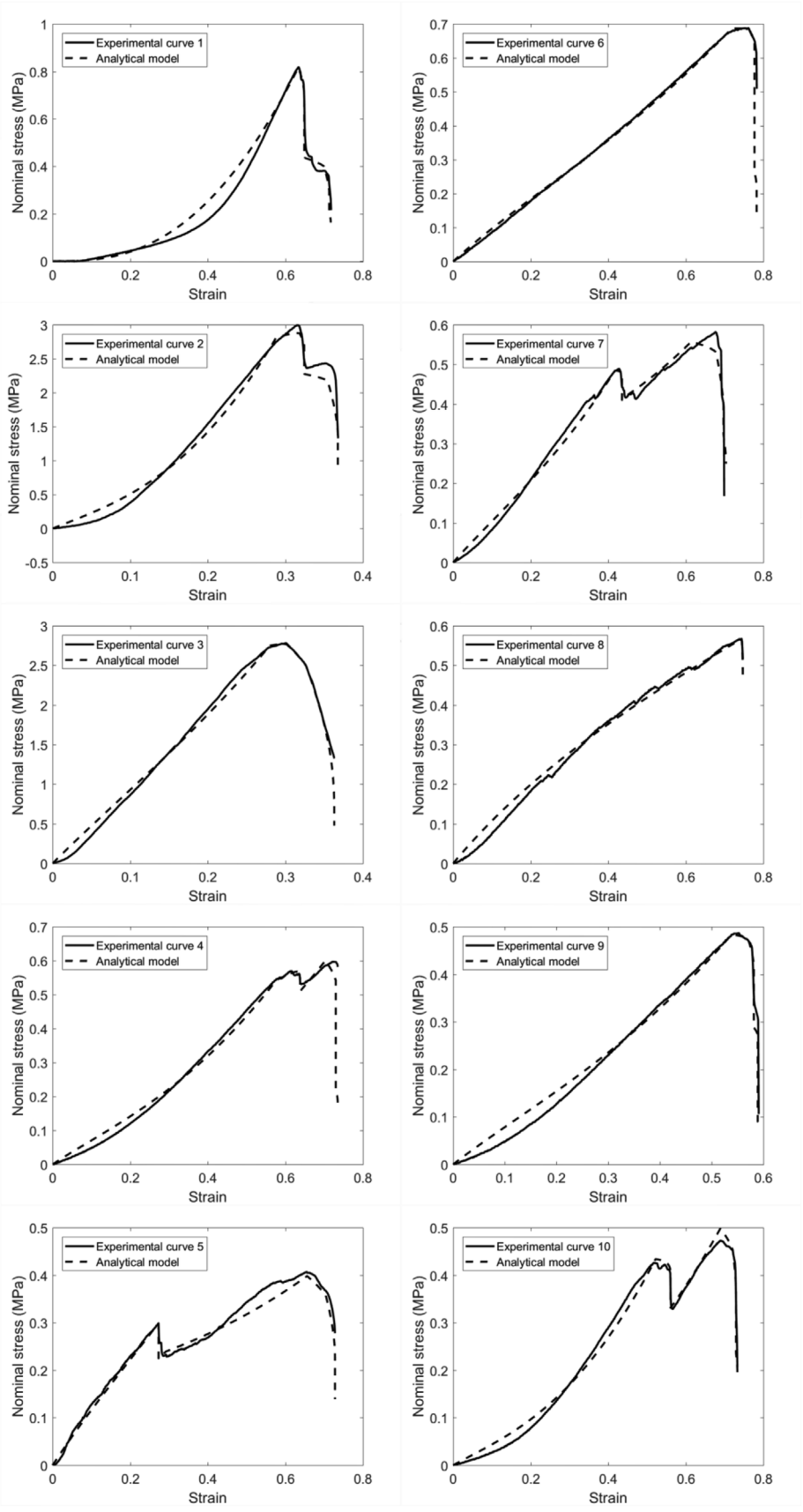

Fig. 6. Comparison between the analytical model (dashed curve) and the experimental tensile test (solid curve). The r^2 are in a range of 0.97–0.99.

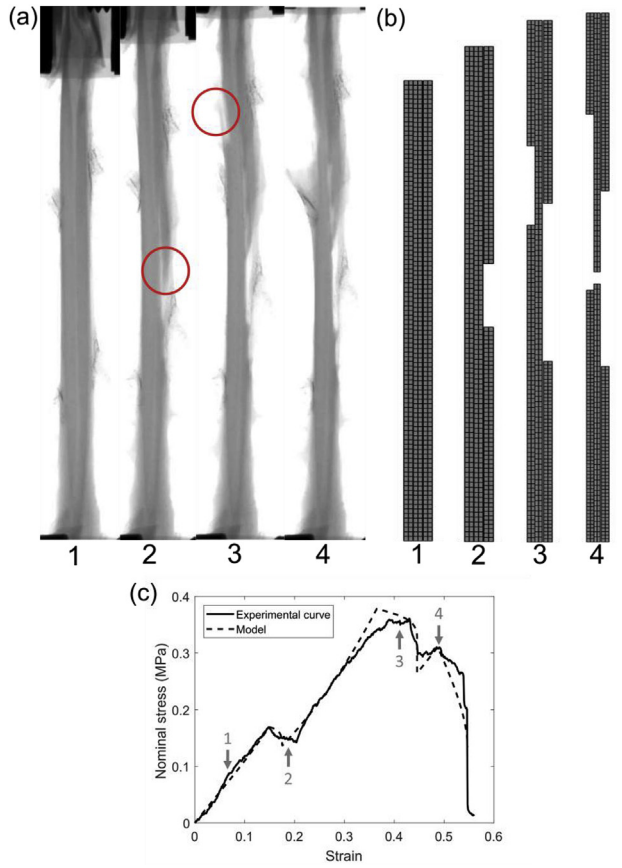

Fig. 7. Analyses of an experimental case. The parameters were identified thanks to the stress-strain curve of the test and the cohesive interfaces were placed in the same configuration as in the X-ray images. (a) Images of the uniaxial tensile test under X-ray tomography at different time steps. The circles highlight the visible sites of ruptures of layers. (b) Images of the finite element model at the same time steps with the parameters corresponding to the case (a). (c) Stress-strain curves of the test (a) and of the model response with the fitted parameters.

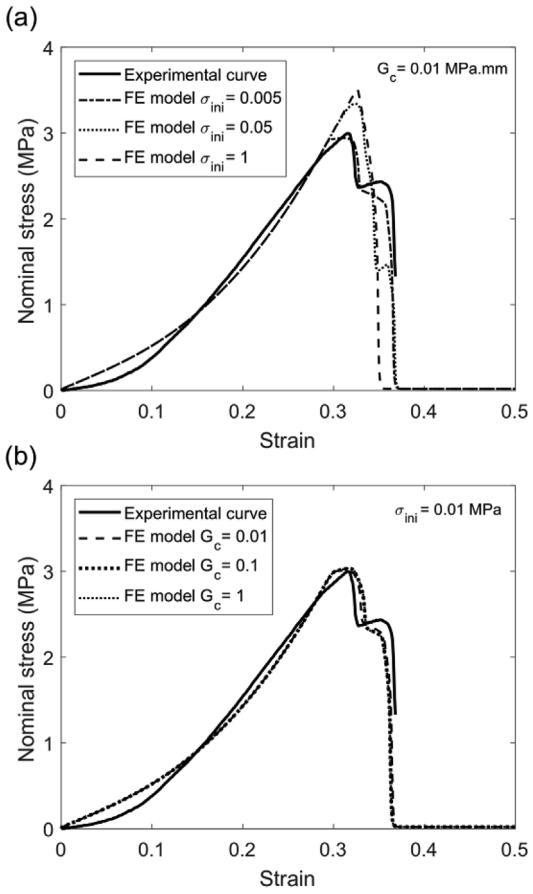

Fig. 8. Comparison of the experiment and the finite element simulations to investigate the influence of the delamination parameters σ_{ini} and G_c. (a) G_c is fixed to 0.01 MPa mm while σ_{ini} varies. When σ_{ini}=0.005 MPa the three layers of the finite element model broke successively like the experiment, when σ_{ini}=0.05 MPa the two first layers of the finite element model broke at the same time and the third layer broke later, and when σ_{ini}=1 MPa the three layers broke at the same time. (b) σ_{ini} is fixed at 0.01 MPa while G_c varies. The three curves are relatively similar, this demonstrates the limited influence of G_c.

of hyper-elasticity and mode I rupture were used as in the analytical model, while for mode II, a sensitivity analysis on the associated values was performed to assess the influence of mode II separation in this mechanical rupture test. The analysis showed that the role of mode II is essential in maintaining layers together. If mode II strength is too high, two adjacent layers would not separate and they would recoil at the same time when the strongest one fails in mode I. Our experiments showed, however, that after breaking in mode I, a layer suddenly recoils and separates from its neighbouring layer in a mode II separation. The combination of these observations suggests that mode II separation may play a major role in crack propagation, as occurring in dissection. More specifically, our model confirmed that a first crack forms due to mode I failure, which then propagates in mode I in the transverse direction until the elastic recoil stress exceeds the mode II strength of a longitudinal plane. The crack will then propagate in the direction of less energy, hence following this plane and forming a delamination plane, as observed clinically and experimentally.

Several studies investigated the mechanisms of dissection using different experiments. Tam et al. (1998) created blebs in the media by injecting saline solution. Sommer et al. (2008), Wang et al. (2014), and Witzenburg et al. (2017) used peeling test (hence mode I longitudinal separation), which are probably more suitable for the analysis of dissection propagation when a relatively long flap is already formed, or for plaque delamination. The present work is believed to be more appropriate for the onset of dissection. Pasta et al. (2012) demonstrated the presence of radially-running fibers of collagen and elastin that create "bridges" between lamellae and support the load induced by delamination. Pal et al. (2014) proposed a predictive mechanistic model that investigated the effect of these fibers and reproduced the response of the peeling tests. The results showed that the number density and failure energy of the radially-running collagen fibers to be the main contributors to the delamination strength. However, the mode of rupture in this study and in the present work are not the same. In the delamination model of Pal et al. (2014), the fibers between the two strips of the peeling test rupture in mode I, whereas in the present model, the different layers separate from each other in mode II. From the present work, it is hypothesized that the separation in mode I between layers would not be activated until a channel is formed and blood rushes into that channel, thus pushing the layers apart. Mode II separation would be the precursor to this channel formation.

As it was shown, delamination is triggered when the recoil of ruptured lamellar units induces shear stress which exceeds mode II strength of the adjacent lamellar unit. Thus, the present study suggests that wall defects may be directly involved in determining the initiation location of the delamination process. Indeed, they could locally weaken this mode II strength. In other words, it is likely that a disease or an intramural hematoma already present at the beginning of the rupture of the intima would promote dissection. It is even possible that the delamination between lamellae has already been propagating when the

intimal tear appears.

Limitations of this work are detailed herein. First, it was based on uniaxial tests, while the *in vivo* loading corresponds to a biaxial or even triaxial stress state. In a study closer to *in vivo* conditions of dissection, this aspect should be considered by implementing a 3D model. Another limitation of the present model based on cohesive zone modeling is that the path of the crack is pre-defined. Here, all experimental observations were consistent regarding the rupture pattern and our cohesive zones were positioned accordingly (transverse and longitudinal). However, in another loading configuration, a different configuration should be considered.

This work provided valuable data toward the characterization of arterial rupture at the lamellar-scale, which could be used in further modeling endeavors. Also, it yielded useful insights into the determinants and conditions that promote dissection *in vivo*. While additional experimental validation is warranted to precisely address *in vivo* dissection conditions, this work opens a way to potentially important clinical applications in monitoring patient-specific vascular risk factors, and management of patients with dissection.

Conflicts of interest

The authors have no conflict of interest.

Acknowledgements

This work was supported by the European Research Council through Starting Grant AArteMIS n°638804.

References

Barenblatt, G.I., 1962. The mathematical theory of equilibrium cracks in brittle fracture. In: Advances in Applied Mechanics. Elsevier, pp. 55–129.
Carson, M.W., Roach, M.R., 1990. The strength of the aortic media and its role in the propagation of aortic dissection. J. Biomech. 23, 579–588.
Dugdale, D.S., 1960. Yielding of steel sheets containing slits. J. Mech. Phys. Solids 8, 100–104.
Ferrara, A., Pandolfi, A., 2010. A numerical study of arterial media dissection processes. Int. J. Fract. 166, 21–33.
Gasser, T.C., Holzapfel, G.A., 2006. Modeling the propagation of arterial dissection. Eur. J. Mech. A Solid. 25, 617–633.
Helfenstein-Didier, C., Taïnoff, D., Viville, J., Adrien, J., Maire, É., Badel, P., 2018. Tensile rupture of medial arterial tissue studied by X-ray micro-tomography on stained samples. J. Mech. Behav. Biomed. Mater. 78, 362–368.
Kouchoukos, N.T., Dougenis, D., 1997. Surgery of the thoracic aorta. N. Engl. J. Med. 336, 1876–1889.
Krasny, W., Morin, C., Magoariec, H., Avril, S., 2017. A comprehensive study of layer-specific morphological changes in the microstructure of carotid arteries under uniaxial load. Acta Biomater. 57, 342–351.
Lagarias, J.C., Reeds, J.A., Wright, M.H., Wright, P.E., 1998. Convergence properties of the Nelder-Mead simplex method in low dimensions. SIAM J. Optim. 9, 112–147.
MacLean, N.F., Dudek, N.L., Roach, M.R., 1999. The role of radial elastic properties in the development of aortic dissections. J. Vasc. Surg. 29, 703–710.
Miao, T., Tian, L., Leng, X., Miao, Z., Xu, C., 2018. A Comparative Study of Cohesive Zone Models for Predicting Delamination Behaviors of Arterial Wall. ArXiv:1806.05785 [q-Bio].
Nienaber, C.A., Clough, R.E., Sakalihasan, N., Suzuki, T., Gibbs, R., Mussa, F., Jenkins, M.T., Thompson, M.M., Evangelista, A., Yeh, J.S.M., Cheshire, N., Rosendahl, U., Pepper, J., 2016. Aortic dissection. Nature Reviews Disease Primers 2, 16053.
Nierenberger, M., Rémond, Y., Ahzi, S., Choquet, P., 2015. Assessing the three-dimensional collagen network in soft tissues using contrast agents and high resolution micro-CT: application to porcine iliac veins. Comptes Rendus Biol. 338, 425–433.
Pal, S., Tsamis, A., Pasta, S., D'Amore, A., Gleason, T.G., Vorp, D.A., Maiti, S., 2014. A mechanistic model on the role of "radially-running" collagen fibers on dissection properties of human ascending thoracic aorta. J. Biomech. 47, 981–988.
Pasta, S., Phillippi, J.A., Gleason, T.G., Vorp, D.A., 2012. Effect of aneurysm on the mechanical dissection properties of the human ascending thoracic aorta. J. Thorac. Cardiovasc. Surg. 143, 460–467.
Rivlin, R.S., 1948. Large elastic deformations of isotropic materials IV. further developments of the general theory. Phil. Trans. Roy. Soc. Lond. 241, 379–397.
Sommer, G., Gasser, T.C., Regitnig, P., Auer, M., Holzapfel, G.A., 2008. Dissection properties of the human aortic media: an experimental study. J. Biomech. Eng. 130, 021007.
Tam, A.S., Catherine Sapp, M., Roach, M.R., 1998. The effect of tear depth on the propagation of aortic dissections in isolated porcine thoracic aorta. J. Biomech. 31, 673–676.
Walton, L.A., Bradley, R.S., Withers, P.J., Newton, V.L., Watson, R.E.B., Austin, C., Sherratt, M.J., 2015. Morphological characterisation of unstained and intact tissue micro-architecture by X-ray computed micro- and nano-tomography. Sci. Rep. 5.
Wang, L., Roper, S.M., Hill, N.A., Luo, X., 2017. Propagation of dissection in a residually-stressed artery model. Biomechanics Model. Mechanobiol. 16, 139–149.
Wang, L., Roper, S.M., Luo, X.Y., Hill, N.A., 2015. Modelling of tear propagation and arrest in fibre-reinforced soft tissue subject to internal pressure. J. Eng. Math. 95, 249–265.
Wang, Y., Johnson, J.A., Spinale, F.G., Sutton, M.A., Lessner, S.M., 2014. Quantitative measurement of dissection resistance in intimal and medial layers of human coronary arteries. Exp. Mech. 54, 677–683.
Witzenburg, C.M., Dhume, R.Y., Shah, S.B., Korenczuk, C.E., Wagner, H.P., Alford, P.W., Barocas, V.H., 2017. Failure of the porcine ascending aorta: multidirectional experiments and a unifying microstructural model. J. Biomech. Eng. 139, 031005.
Wolinsky, H., Glagov, S., 1967. A lamellar unit of aortic medial structure and function in mammals. Circ. Res. 20, 99–111.